Nanoscale

Accepted Manuscript

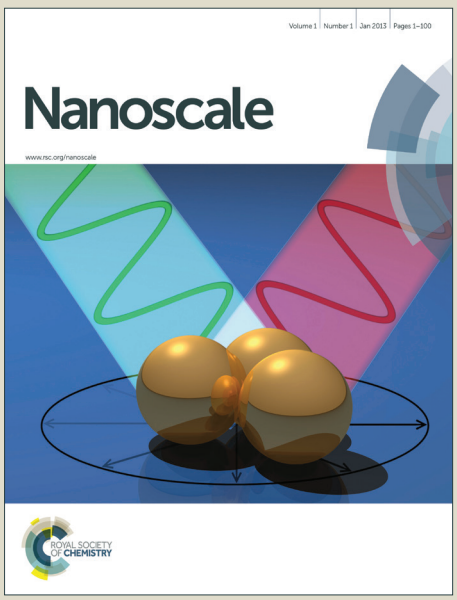

ROYAL SOCIETY OF CHEMISTRY

www.rsc.org/nanoscale

Nanoscale

COMMUNICATION

2D Ultrathin Core-shell Pd@Pt$_{monolayer}$ Nanosheets: Defect-Mediated Thin Film Growth and Enhanced Oxygen Reduction Performance

Received 00th January 20xx,
Accepted 00th January 20xx

DOI: 10.1039/x0xx00000x

www.rsc.org/

Wenxin Wang,[a,b] Yunfeng Zhao*[a] and Yi Ding*[a]

An operational strategy for the synthesis of atomically smooth Pt skin by a defect-mediated thin film growth method is reported. Extended ultrathin core-shell structured Pd@Pt$_{monolayer}$ nanosheets (thickness below 5 nm) exhibit a seven-fold enhancement in mass-activity and surprisingly good durability toward oxygen reduction reaction as compared with the commercial Pt/C catalyst.

Proton exchange membrane fuel cells (PEMFCs) represent one of the ideal low emission and efficient power resources. However, the successful application of PEMFCs has long been restricted by three major criteria: price, performance and durability[1]. The pivotal component is the electrocatalyst system that underpins fuel-cell operation[1,2], and the commercial carbon supported platinum nanoparticle (Pt/C) catalyst typically contributes more than one third of the overall fuel cell stack cost[3]. Compared to the relatively fast reaction kinetics of hydrogen oxidation on the anode side, a majority of Pt is required at the cathode to catalyze the inherently sluggish oxygen reduction reaction (ORR)[4-6]. The recent progress in surface science has contributed to better understanding of reaction mechanisms on catalysts and appropriately arranged surface structures are key to the next generation high performance ORR catalysts[7-10]. For example, extended (110) and (111) Pt crystal planes were found to be far more active than (100) plane and those less ordered surfaces as often found in most nanostructures, especially in perchloric acid[11]. Alloying the surface or near surface region of Pt catalysts with other elements is another effective strategy to enhance the intrinsic surface activity of Pt-based ORR catalysts[10, 12-14]. Therefore, it is highly challenging to design a high surface area Pt electrocatalyst that shows both intrinsic activity and long term durability.

Core-shell type nanostructures, especially those with a monolayer Pt skin, often exhibit higher mass activities due to enhanced Pt utilization and at the same time the substrate material provides additional advantageous modification of the electronic structures of the surface Pt atoms[1,11,15-17]. For example, Pd substrate was reported to be able to lower the Pt surface oxygen affinity, which is beneficial to its ORR activity[15]. Current efforts on Pt skin ORR catalysts focus mostly on core-shell nanoparticulate materials, whose enhanced performance was often ascribed to the lattice contraction effect[18] or the exposure of high-index facets[19,20]. The explanations, however, are not in complete consistency with fundamental electrochemical understanding of Pt-based electrodes which predicts that highly *nanostructured* Pt surfaces (such as decreased dimension and high-index facets) are *not* favorable for ORR because they often exhibit stronger binding to the oxygenated intermediates[11]. The observed activity enhancement could be due to intricate interplays among many factors such as Pt utilization and alloying effect. In this regard, it is of great interest to fabricate two dimensional core-shell nanocatalysts with atomically thin and flat Pt surfaces. In this configuration, the extended Pt surface lattices and the underlying substrate material could simultaneously contribute to the enhanced intrinsic activity of Pt by weakening the adsorption strength of oxygen species, while the ultrathin Pt overlayer guarantees the overall Pt utilization.

To fabricate an atomically thin and smooth overlayer on a foreign substrate, the traditional seeding growth[21] and vapor deposition[22] methods are not readily applicable because the Pt outer shell thus produced often exhibits island morphology with at least several atomic layer thickness[23]. Underpotential deposition (UPD) of Cu followed by galvanic replacement has been regarded as one of the best choices for synthesizing monolayer type shell structures[24,25], but this process relies on the successful establishment of a thermodynamic couple between the foreign admetal and the substrate, which is not always existent[26]. Therefore, it is desirable to develop reliable techniques that allow generation of uniform metal adlayers with controllable layer thickness at atomic scale and under moderate circumstances. These techniques would provide a versatile platform for both fundamental research and practical investigations, in particular for the development of

[a] *Institute for New Energy Materials & Low-Carbon Technologies, School of Materials Science and Engineering, Tianjin University of Technology, Tianjin 300384, China. Email: yding@tjut.edu.cn, yunfeng.zhao@kaust.edu.sa; Tel: +86-22-60216546*

[b] *Center for Advanced Energy Materials & Technology Research (AEMT), School of Chemistry and Chemical Engineering, Shandong University, Jinan 250100, China.*

† Electronic Supplementary Information (ESI) available: Sample preparation, physical and electrochemical characterization, Figures S1 to S11.
See DOI: 10.1039/x0xx00000x

unique catalyst systems with novel structural properties for advanced energy technologies such as ORR.

Defect-mediated thin-film growth (DMTFG) can manage to deposit an element under an overpotential environment with the help from Cu or Pb underpotential deposition/stripping cycles into the monolayer or bilayer structure[27], and this method has been reported to synthesize monolayer structure on nanoparticles[28]. To the best of our knowledge, it is rare to adopt this method to manipulate ultrathin nanoplate surfaces. Considering the positive effect of Pd substrates on the improvement of ORR activity of Pt[29,30], in this work, we develop a modified DMTFG method to generate ultrathin core-shell Pd@$Pt_{monolayer}$ nanoplate electrocatalysts (Scheme 1a). These novel catalysts effectively coordinate the utilization maximization of precious Pt atoms with the positive electronic perturbation from the Pd substrate[15,31,32], which in turn lead to their dramatically enhanced ORR performance.

The ultrathin palladium nanoplates with an average diameter of 200 nm and height of 5 nm were prepared by thermal reduction of palladium acetylacetonate ($Pd(acac)_2$) by a mixture of benzyl alcohol, cetyltrimethylammonium bromide (CTAB) and polyvinylpyrrolidone (PVP) in the presence of CO at 70 ^{o}C, a colloidal method first reported by Zheng and co-workers (Fig. S1)[33]. The dissolved CO molecules provide a bi-functional effect in a way that bridge adsorbed CO molecules on the Pd basel (111) facet has strong electronic confinement effect which helps the anisotropic growth of ultrathin hexagonal Pd nanoplates[34,35]. The face-centered cubic (fcc) structure with a cell parameter a=3.89 Å of as-prepared Pd nanoplates was determined by powder X-ray diffraction (XRD) pattern (JCPDS no. 46-1043) as illustrated in Fig. S2. In order to remove the surfactants and polymer molecules adsorbed on the surface of Pd nanoplates, an electrochemical method was utilized to by potential sweeping from 0.2-1.2 V (scan speed 10 mV s^{-1}) in acidic medium, which facilitated the revealing of pristine single crystalline surface of Pd nanoplates[36,37]. The evidently increased hydrogen adsorption/desorption peak (0.2-0.35 V)[38] in the second scan as compared with the completely suppressed peak signal in the first scan signifies this successful surface clean process (Fig. S3a). Careful electrochemical characterization revealed further interesting behavior of these ultrathin Pd nanoplates. As shown in Fig. S3b, this electrochemical cleaning process allowed the exposure of more Pd (110) facet[38]. And upon structure inheritage by an epitaxial Pt surface layer, this extended facet structure will be highly beneficial to the enhanced ORR activity, especially in perchloric acid[39]. Interestingly, these clean Pd nanoplates already demonstrated impressive ORR activity (Fig. S4), although it is well known that the durability of pure Pd nanostructures upon continuous potential cycling in acidic medium is quite poor.

We then developed a DMTFG method to generate an epitaxial Pt overlayer on Pd nanoplates (Scheme 1b). Instead of UPD at a fixed potential, this method involves Cu UPD and stripping to modify the growth kinetic of the Pt film which lowered the rate of Pt deposition and enhanced surface diffusion of Pt adatoms to form a smooth monolayer[27]: the metal of interest (Pt) co-deposits with a reversibly deposited mediator metal (Cu) which is periodically deposited and stripped from the surface by cycling the electrochemical potential. The monolayer Pt formation can be understood by the following mechanism: 1) Cu adatoms are first deposited on the Pd surface, forming high density 2D Cu nuclei that serve as attachment sites for Pt adatoms on the surface; 2) rapid interlayer exchange minimizes intralayer adatom diffusion; 3) on the reverse portion of the cycle, Cu selectively stripped from the surface causes the Pt-Cu 2D clusters to decompose into 2D Pt islands that serve as growth centers as Pt continues to deposit. During the entire process, Cu UPD layer behaves as a significant surfactant by promoting interlayer terrace exchange between deposited Pt adatoms and mediate atoms. The effectiveness of Cu UPD mediator can also be appreciated by the suppressed Pd stripping by the involvement of Cu electrochemistry as shown in Fig. S5.

This monolayer structure can be characterized by atomic force microscopy (AFM). After Pt monolayer deposition on the Pd nanoplates (Fig.1a &1b), the average height changed from 4.1 ± 0.1 nm to 4.7 ± 0.1nm. Considering the atom diameter (2.77 Å) and lattice constant(3.92 Å) of Pt, the increased 6 Å stands for a total of 2.16 layers which were deposited on the top and bottom sides of the Pd nanoplate substrate, equivalent to 1.08 atomic layer of Pt on each side. The successful synthesis of Pt monolayer can also be indicated from the CO stripping. As shown in Fig. S6, the CO

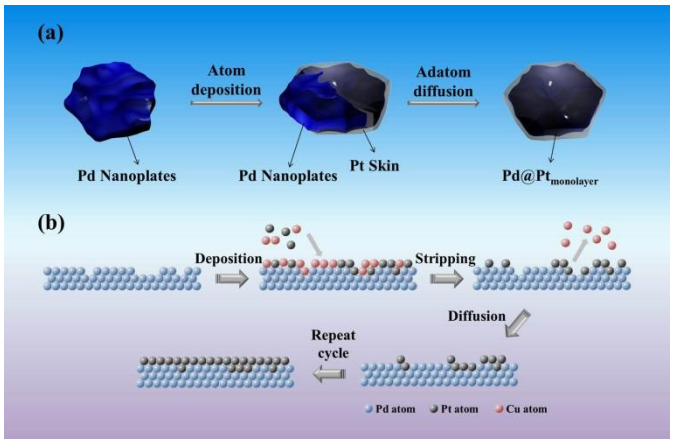

Scheme 1(a) Schematic representation of the morphology change steps of Pd@$Pt_{monolayer}$ during surface modification. (b) Schematic diagram of the DMTFG method.

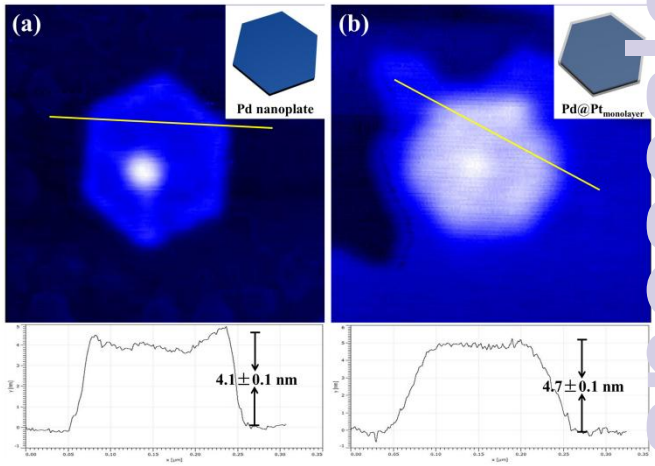

Fig.1 AFM images of (a) pure Pd substrate and (b) $Pd_{@}Pt_{monolayer}$ with the height details at yellow region.

stripping peak of Pd@$Pt_{monolayer}$ catalyst shifts towards higher potential as compared with that of Pt/C, while those characteristic CO stripping peaks from the original Pd nanoplates also vanish significantly. This indicates an electronic alteration (reduction) of Pt Fermi level local density of states by the Pd substrate[40], which helps the reduction of OH adsorption and improves its ORR catalysis capability. Additional characters about structure and composition of Pd@$Pt_{monolayer}$ ultrathin nanoplate catalysts were obtained by high-resolution TEM (HRTEM), high-angle annular dark field STEM (HAADF-STEM), energy-dispersive X-ray (EDX) mapping and X-ray photoelectron spectroscopy (XPS). After deposition, the ultrathin plate structure kept the same as the Pd substrate[33]. 1/3 (422) reflection SAED pattern (Fig. S7) was observed on the Pd@$Pt_{monolayer}$, which comes from the Pd substrate with a stacking fault parallel to the basal (111) planes in an fcc plate structure[41,42]. The lattice fringes (Fig. 2c&d) with the interplanar spacing of 2.4 and 2.2Å have a good agreement with the Pd substrate. HAADF-STEM-EDS (Fig.2b) was used to analyze the component distribution of Pd and Pt after surface modification, which gives an atomic ratio of 19:1 between Pd and Pt. XPS results (Fig. S8) provide the information about the core-level Pd 3*d* spectra of Pd@$Pt_{monolayer}$ with peak signals at 340.8 and 335.6 eV for Pd $3d_{3/2}$ and Pd $3d_{5/2}$, respectively. Compared with the standard pure Pd 3*d* signals of 340.3 eV (Pd $3d_{3/2}$) and 335.0 eV (Pd $3d_{5/2}$)[43], substrate Pd has a slight upshift of binding energy which could be ascribed to the electron transfer between Pd and Pt[44]. Slightly lower shift of Pt 4*f* core-level spectra of Pd@$Pt_{monolayer}$, as compared with pure Pt (74.4 eV for $4f_{5/2}$ and 71.0 eV for Pt $4f_{7/2}$), also points to certain electron transfer from Pd to Pt.

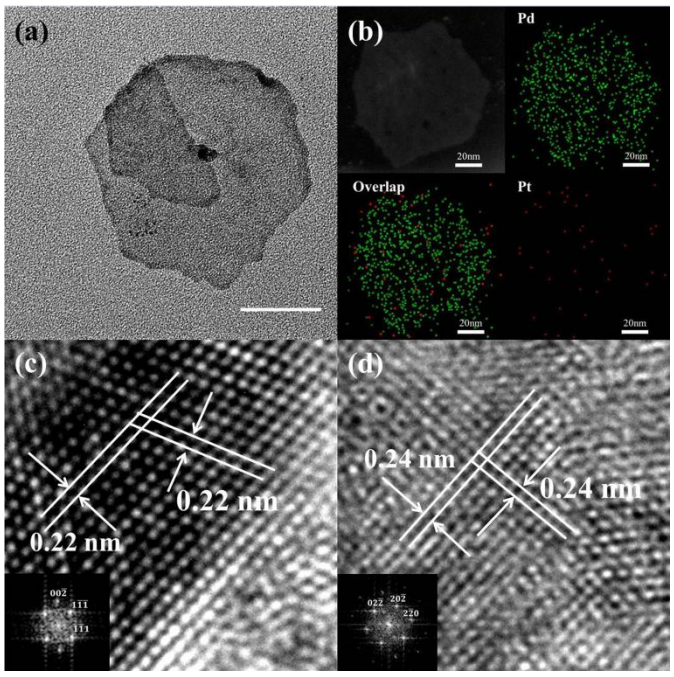

Fig.2 (a) TEM image of Pd@$Pt_{monolayer}$, the scale bar stands for 40 nm. (b) HAADF-STEM image of Pd@$Pt_{monolayer}$. Pd and Pt elements were showed as green and red, respectively. (c, d) HRTEM images of a Pd@$Pt_{monolayer}$ recorded from the [110] and [111] zone orientation, respectively. Insets are the SAED patterns.

Interestingly, after the deposition treatment, we found the surface roughness showed an obvious trend of becoming smoother based on the AFM analyses. After deposition of Pt monolayer on the Pd nanoplates (Fig. S9), the average roughness (R_a) and root mean square roughness (R_q) of Pd@$Pt_{monolayer}$ are 0.19 and 0.25 nm respectively, both of which are lower than those of Pd substrate (R_a 0.26, R_q 0.32). This provides additional evidence for the DMTF mechanism that the copper mediator helps the Pt adatoms diffuse into a thermodynamically stable structure with more smooth surfaces.

According to the literatures, facets (110) and (111) of Pd electrodes possess the higher catalytic ability among low index facets in perchloric acid[34]. By inheriting these preferential facets from the Pd nanoplates (Fig.2d), Pd@$Pt_{monolayer}$ is highly promising as an active ORR electrocatalysts. Cyclic voltammogram (CV) features its positively shifted on-set potentials for the redox waves of Pt in Pd@$Pt_{monolayer}$ as compared with Pt/C (Fig.3a), suggesting the delayed formation and weakening of Pt-oxygenated species after alloying with the Pd substrate, which is typically a desired feature for a good ORR catalyst. At the same time, Pd@$Pt_{monolayer}$ demonstrates much broader electrochemical signals, especially in the hydrogen region, reminiscent of the rich hydrogen adsorption/absorption behavior of Pd-based electrodes. ORR polarization curves for Pd@$Pt_{monolayer}$, pure Pd substrate and commercial Pt/C were measured in 0.1 M oxygen-saturated perchloric acid electrolyte at 30 °C (Fig.3b). Besides the enhanced electrochemical surface area ($ECSA_{Pd@Ptmonolayer}$ = 171.45 m^2 g_{Pt}^{-1} and $ECSA_{Pt/C}$ = 77.96 m^2 g_{Pt}^{-1}), Pd@$Pt_{monolayer}$ (0.874 V) exhibits 22 mV higher half-wave potential as compared with Pt/C (0.852 V), which proves the improvement of ORR reaction kinetics at lower over-potential. The kinetic activity was further investigated by Tafel plots at the mixed kinetic-diffusion control region (0.8-1.0 V). According

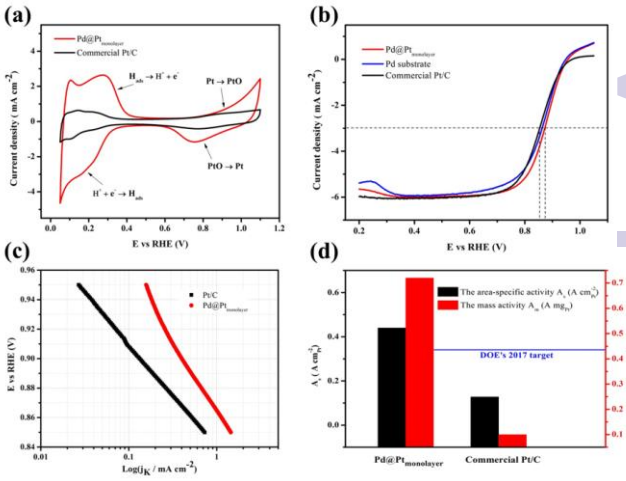

Fig. 3 (a) CV profiles of Pd@$Pt_{monolayer}$ and Pt/C catalysts in N_2 purged 0.1 M $HClO_4$ solution at room temperature. Scan rate: 50 mV s^{-1}. (b) Polarization curves (anodic sweep direction) for Pd@$Pt_{monolayer}$, Pd substrate and Pt/C immobilized onto a glassy carbon rotating disk electrode obtained at a rotation rate of 1600 rpm in a 0.1 M O_2 purged $HClO_4$ solution at 30 °C, scan rate 10 mV s^{-1}. (c) The area-specific kinetic current densities (j_K) for Pd@$Pt_{monolayer}$ and commercial Pt/C. (d) The area and mass specific activity kinetic current densities for Pd@$Pt_{monolayer}$ and Pt/C at 0.9 V.

to Fig.3c, in the whole potential region, Pd@$Pt_{monolayer}$ shows enhanced kinetic activities. At 0.9 V, its area-specific activity (A_s) reaches 0.438 A cm_{Pt}^{-2}, while its mass activity (Am) was calculated to be 0.717 A mg_{Pt}^{-1} (Fig.3d). Compared with the commercial Pt/C catalyst (A_s = 0.128 A cm_{Pt}^{-2}, A_m = 0.109 A mg_{Pt}^{-1}), Pd@$Pt_{monolayer}$ exhibits an enhancement factor of 3.4 and 6.6 for A_s and A_m, respectively. These results approach the US DOE 2017 target for Pt based ORR catalysts (A_m = 0.44 A mg_{Pt}^{-1})[1].

As a vital property for PEMFC application, the catalytic durability of Pd@$Pt_{monolayer}$ was measured by accelerated durability test (ADT), i.e., continuous potential sweeps between 0.6 and 1.0 V in oxygen-saturated 0.1 M $HClO_4$ solution for 5000 cycles at a scan rate 50 mV s^{-1} at 30 ^oC. Upon long-time cycling, the ORR activity of Pd@$Pt_{monolayer}$ only shows a negative shift of 18 mV for half-wave potential (Fig.4a), which is significantly better than Pt/C's 59 mV potential decrease (Fig.4b). The morphological evolution of as-prepared Pd@$Pt_{monolayer}$ and Pt/C was monitored by TEM (Figures S10 and S11). Upon durability test, Pt/C was found to have undergone significant Ostwald ripening and its morphology has changed from an original state of relatively uniform dispersion of 3 nm Pt particles on carbon support, to severely aggregated 10-30 nm particles. The destabilization of Pt/C is also related to the weak interaction between Pt nanoparticles and carbon support[45,46]. For supportless Pd@$Pt_{monolayer}$, the catalysts well retain the hexagonal morphology of the native Pd nanoplates before the durability test (Fig. S11). Upon 5000 times potential cycling, these hexagonal nanoplates transform into less defined porous structure although its overall nanoplate morphology still exists. The main driving force should be related to the dissolution of the less stable Pd substrate[47]. The dark spots formed on the surface might be the locally segregated platinum species whose exact structure requires further characterization. The formation of porous structure has to be accompanied by the exposure of more Pd atoms from underneath. And the porous structure formation may contribute to favorable mass transport and higher surface area, which would counteract the activity loss due to the degradation of the core-shell type nanoplates. Indeed, from the hydrogen adsorption/desorption region, we did not observe any noticeable decrease in overall charge involved. The slight decrease for the current density at around 0.1 V is balanced by an increase of a more characteristic peak at ~0.2 V, indicative of the incorporation of more Pd electrochemical signals.

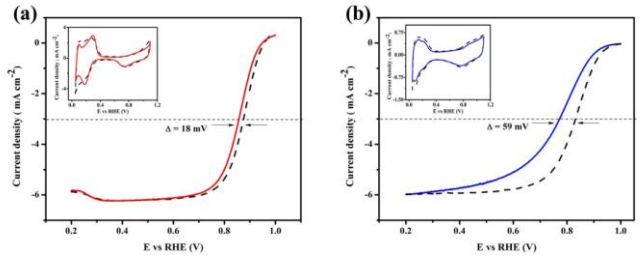

Fig.4 ORR polarization curves for (a) Pd@$Pt_{monolayer}$ and (b) Pt/C before (dash line) and after (solid line) 5000 potential sweeps in O_2-saturated 0.1 M $HClO_4$ solution at a scan rate 10 mV s^{-1}. Insets features the respective CV plots upon 5000 potential sweeps in N_2-saturated 0.1 M $HClO_4$ solution at a scan rate 50 mV s-1.

Conclusions

In summary, ultrathin core-shell Pd@$Pt_{monolayer}$ nanosheets were successfully synthesized by a defect-mediated thin film growth method on Pd substrate which showed outstanding catalytic activity and stability toward the oxygen reduction reaction in acidic electrolyte. This process allows careful tuning of the surface smoothness of the plate-like core-shell nanostructures, which was monitored by atomic force microscopy. The benefits from these unique quasi-two-dimensional core-shell nanoplates with a smooth and atomically thin skin can be appreciated by their evidently enhanced area-specific and mass activities, which are better than the commercial Pt/C by a factor of 3.4 and 7, respectively. Although long term durability test could also damage its core-shell plate like morphology, supportless Pd@$Pt_{monolayer}$ was found to be significantly durable than supported Pt/C upon 5000 times ADT cycling. This work provides a unique strategy for the fabrication of atomically smooth and thin overlayer nanostructures, which allow simultaneous enhancement of mass specific activity and Pt utilization. And this electrode design concept may be applicable to other new materials used for a wide variety of energy technologies.

Acknowledgements

This research was supported by the National 973 Program Project of China (2012CB932800), the National Science Foundation of China (51171092), and the Ph.D. Program Foundation of the Chinese Ministry of Education (MOE 20120042110031). Y. D. also acknowledges the Fundamental Research Funds of Shandong University.

Notes and references

1. M. K. Debe, *Nature*, 2012, **486**, 43-51.
2. F. T. Wagner, B. Lakshmanan and M. F. Mathias, *J. Phys. Chem. Lett.*, 2010, **1**, 2204-2219.
3. J. K. Brian D. James, Kevin Baum, *Department of Energy Hydrogen Program Review*, 2011.
4. D. C. Higgins, R. Wang, M. A. Hoque, P. Zamani, S. Abureden and Z. Chen, *Nano Energy*, 2014, **10**, 135-143.
5. J. Zhang, *PEM fuel cell electrocatalysts and catalyst layers: fundamentals and applications*, Springer, 2008.
6. A. Wieckowski, *Fuel cell catalysis: a surface science approach*, John Wiley & Sons, 2009.
7. J. Wu and H. Yang, *Acc. Chem. Res.*, 2013, **46**, 1848-1857.
8. J. Zhang, M. B. Vukmirovic, K. Sasaki, A. U. Nilekar, M. Mavrikakis and R. R. Adzic, *J. Am. Chem. Soc.*, 2005, **127**, 12480-12481.
9. D. Wang, H. L. Xin, Y. Yu, H. Wang, E. Rus, D. A. Muller and H. D. Abruña, *J. Am. Chem. Soc.*, 2010, **132**, 17664-17666.
10. G. Wang, B. Huang, L. Xiao, Z. Ren, H. Chen, D. Wang, H. D. Abruña, J. Lu and L. Zhuang, *J. Am. Chem. Soc.*, 2014, **136**, 9643-9649.
11. H. A. Gasteiger and N. M. Marković, *Science*, 2009, **324**, 48-49.

12. H. Zhang, X.-K. Gu, C. Canlas, A. J. Kropf, P. Aich, J. P. Greeley, J. W. Elam, R. J. Meyers, J. A. Dumesic, P. C. Stair and C. L. Marshall, *Angew. Chem., Int. Ed.*, 2014, **53**, 12132-12136.
13. X. Zhao, S. Chen, Z. Fang, J. Ding, W. Sang, Y. Wang, J. Zhao, Z. Peng and J. Zeng, *J. Am. Chem. Soc.*, 2015, **137**, 2804-2807.
14. B. Xia , H. Wu , Y. Yan , X. Lou and X. Wang, *J. Am. Chem. Soc.*, 2013, **135**, 9480-9485.
15. J. K. Nørskov, J. Rossmeisl, A. Logadottir, L. Lindqvist, J. R. Kitchin, T. Bligaard and H. Jónsson, *J. Phys. Chem. B*, 2004, **108**, 17886-17892.
16. K. Sasaki, H. Naohara, Y. Choi, Y. Cai, W.-F. Chen, P. Liu and R. R. Adzic, *Nature Commun.*, 2012, **3**, 1115.
17. C. Koenigsmann, A. C. Santulli, K. Gong, M. B. Vukmirovic, W.-p. Zhou, E. Sutter, S. S. Wong and R. R. Adzic, *J. Am. Chem. Soc.*, 2011, **133**, 9783-9795.
18. J. X. Wang, C. Ma, Y. Choi, D. Su, Y. Zhu, P. Liu, R. Si, M. B. Vukmirovic, Y. Zhang and R. R. Adzic, *J. Am. Chem. Soc.*, 2011, **133**, 13551-13557.
19. Q. Zhang and H. Wang, *ACS Catal.*, 2014, 4027-4033.
20. Z.-Y. Zhou, Z.-Z. Huang, D.-J. Chen, Q. Wang, N. Tian and S.-G. Sun, *Angew. Chem., Int. Ed.*, 2010, **49**, 411-414.
21. X. Xia, L. Figueroa-Cosme, J. Tao, H.-C. Peng, G. Niu, Y. Zhu and Y. Xia, *J. Am. Chem. Soc.*, 2014, **136**, 10878-10881.
22. D. V. Esposito, S. T. Hunt, A. L. Stottlemyer, K. D. Dobson, B. E. McCandless, R. W. Birkmire and J. G. Chen, *Angew. Chem., Int. Ed.*, 2010, **49**, 9859-9862.
23. Y. Ding, M. Chen and J. Erlebacher, *J. Am. Chem. Soc.*, 2004, **126**, 6876-6877.
24. B. Xia , H. Wu , X. Wang and X. Lou , *J. Am. Chem. Soc.*, 2012, **134**, 13934–13937.
25. B. Xia, H. Wu, N. Li, Y. Yan, X. Lou and X. Wang, *Angew. Chem., Int. Ed.*, 2015, **54**, 3797-3801.
26. S. Brimaud and R. J. Behm, *J. Am. Chem. Soc.*, 2013, **135**, 11716-11719.
27. K. Sieradzki, S. R, Brankovic and N. Dimitrov, *Science*, 1999, **284**, 138-141.
28. J. X. Wang, H. Inada, L. Wu, Y. Zhu, Y. Choi, P. Liu, W.-P. Zhou and R. R. Adzic, *J. Am. Chem. Soc.*, 2009, **131**, 17298-17302.
29. Y. Cai and R. Adzic, *Adv. Phys. Chem.*, 2011, 530397-530413.
30. J. Zhang, M. B. Vukmirovic, K. Sasaki, F. Uribe and R Adzic, *J. Serb. Chem. Soc*, 2005, **70**, 513-525.
31. K. Sasaki, J. X. Wang, H. Naohara, N. Marinkovic, K. More, H. Inada and R. R. Adzic, *Electrochim. Acta*, 2010, **55**, 2645-2652.
32. H. Zhang, M. Jin and Y. Xia, *Chem. Soc. Rev.*, 2012, **41**, 8035-8049.
33. X. Huang, S. Tang, X. Mu, Y. Dai, G. Chen, Z. Zhou, F. Ruan, Z. Yang and N. Zheng, *Nature Nanotech.*, 2011, **6**, 28-32.
34. Z. Zhang, Q. Niu and C.-K. Shih, *Phys. Rev. Lett.*, 1998, **80**, 5381-5384.
35. R. Jin, Y. Charles Cao, E. Hao, G. S. Metraux, G. C. Schatz and C. A. Mirkin, *Nature*, 2003, **425**, 487-490.
36. H. Ataee-Esfahani, M. Imura and Y. Yamauchi, *Angew. Chem., Int. Ed.*, 2013, **52**, 13611-13615.
37. H. Ataee-Esfahani, J. Liu, M. Hu, N. Miyamoto, S. Tominaka, K. C. W. Wu and Y. Yamauchi, *Small*, 2013, **9**, 1047-1051.
38. M. Hara, U. Linke and T. Wandlowski, *Electrochim. Acta*, 2007, **52**, 5733-5748.
39. N. Markovic, H. Gasteiger and P. N. Ross, *J. Electrochem. Soc.*, 1997, **144**, 1591-1597.
40. P. K. Babu, H. S. Kim, J. H. Chung, E. Oldfield and A. Wieckowski, *J. Phys. Chem. B*, 2004, **108**, 20228-20232.
41. V. Germain, J. Li, D. Ingert, Z. L. Wang and M. P. Pileni, *J. Phys. Chem. B*, 2003, **107**, 8717-8720.
42. R. Jin, Y. Cao, C. A. Mirkin, K. L. Kelly, G. C. Schatz and J. G. Zheng, *Science*, 2001, **294**, 1901-1903.
43. L. S. Kibis, A. I. Titkov, A. I. Stadnichenko, S. V. Koscheev and A. I. Boronin, *Appl. Surf. Sci.*, 2009, **255**, 9248-9254.
44. F. Tao, M. E. Grass, Y. Zhang, D. R. Butcher, J. R. Renzas, Z. Liu, J. Y. Chung, B. S. Mun, M. Salmeron and G. A. Somorjai *Science*, 2008, **322**, 932-934.
45. R. Wang, C. Xu, X. Bi and Y. Ding, *Energy Environ. Sci.*, 2012, **5**, 5281-5286.
46. R. Borup, J. Meyers, B. Pivovar, Y. S. Kim, R. Mukundan, N. Garland, D. Myers, M. Wilson, F. Garzon and D. Wood, *Chem. Rev.*, 2007, **107**, 3904-3951.
47. K. Sasaki, H. Naohara, Y. Cai, Y. M. Choi, P. Liu, M. B. Vukmirovic, J. X. Wang and R. R. Adzic, *Angew. Chem., Int. Ed.*, 2010, **49**, 8602-8607.